

**CALCULATION OF THE NONSTATIONARY, NONLINEAR  
THREE-DIMENSIONAL PROBLEM OF HEAT CONDUCTION  
BY THE FINITE-ELEMENT METHOD IN CONTINUOUS  
LASER HEATING**

**E. I. Degtyarev**

UDC 536.2

*The process of nonstationary high-intensity laser surface heating of a three-dimensional body in the shape of a rectangular parallelepiped by a continuous laser with a normal distribution of the power density in the heating spot has been investigated numerically with the finite-element method. Consideration has been given to the process of formation of the heat-affected zone and its geometry. Thermal cycles of zonal points and their characteristics have been investigated.*

**Mathematical Model.** In constructing a mathematical model of the process of laser surface thermal hardening of carbon-iron steels [1, 2], one must analyze time changes in the temperature field (thermal cycles) of points of the heat-affected zone in the process of laser heating.

We consider a variant of solid-phase hardening (without fusing the surface) by a continuous laser. The laser source will be represented in the approximation of a distributed surface heat source, while the process of interaction of laser radiation with a substance will be represented as the process of heating. The scheme of thermal loading is shown in Fig. 1a. For the most adequate results we will employ numerical methods, the most efficient of which is the finite-element method.

The temperature distribution in the body under study is described by the parabolic heat-conduction equation [3]

$$c_v \rho \frac{\partial T}{\partial t} = \text{div} (\lambda \text{ grad } T), \tag{1}$$

where  $\rho(x^i)$ ,  $c_v(x^i, T)$ , and  $\lambda(x^i, T)$  are the density, the specific heat at constant volume, and the symmetric second-rank tensor of thermal conductivity of the material with components  $\lambda_{ij}$  ( $i, j = 1, 2, 3$ ) respectively. The initial condition for Eq. (1) has the following form:

$$T(x^i, t) |_{t=0} = T_0(x^i). \tag{2}$$

We will assume that a distributed surface heat source with a normal distribution of the (flux) power density in the heating spot, which moves uniformly and rectilinearly along the coordinate direction  $x^2$  with velocity  $\mathbf{V}$ , is acting on the body's surface  $x^3 = 0$ . With allowance for this fact we represent the boundary conditions (of the second, third, and fourth kind) as

$$\begin{aligned} x^1 = 0: & \quad q_1 = 0; \quad x^1 = L_1: q_1 = q_{\text{conv}} + q_{\text{rdnt}}; \\ x^2 = 0: & \quad q_2 = -q_{\text{conv}} - q_{\text{rdnt}}; \quad x^2 = L_2: q_2 = q_{\text{conv}} + q_{\text{rdnt}}; \\ x^3 = 0: & \quad q_3 = q_{\text{las.r}} - q_{\text{conv}} - q_{\text{rdnt}}; \quad x^3 = L_3: q_3 = q_{\text{conv}} + q_{\text{rdnt}}, \end{aligned} \tag{3}$$

---

N. É. Bauman Moscow State Technical University, Moscow, Russia; email: degtyarev@box.vsi.ru. Translated from *Inzhenerno-Fizicheskii Zhurnal*, Vol. 76, No. 6, pp. 156–160, November–December, 2003. Original article submitted September 17, 2002; revision submitted March 24, 2003.

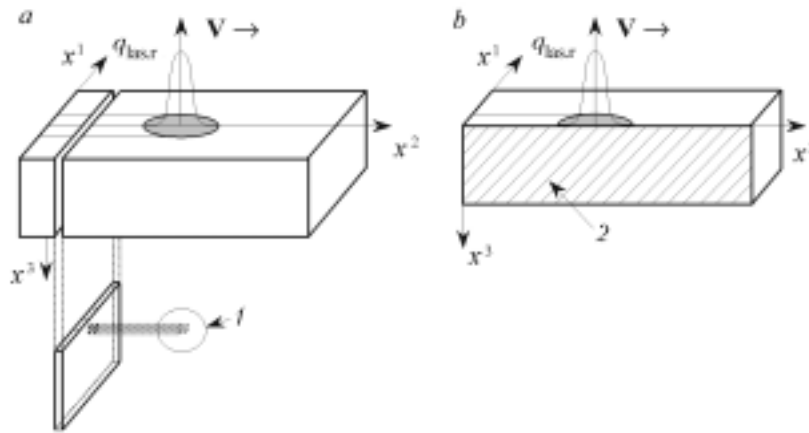


Fig. 1. Scheme of thermal loading of a body (a) and calculation region (b): 1) microvolume under study (individual point of a continuum); 2) adiabatic boundary (by virtue of the symmetry of the calculation region).

TABLE 1. Characteristics of the Calculation Region (material 45 steel)

Parameters	$x^1$	$x^2$	$x^3$
Linear dimensions, mm	3	5	2
Number of finite elements	20	40	20
Type of grid	Tangential	Uniform	Tangential

where  $q_{\text{conv}} = \alpha(T(x^i, t) - T_{\text{amb.m}})$ ,  $q_{\text{rdnt}} = \sigma \varepsilon (T^4(x^i, t) - T_{\text{amb.m}}^4)$ ,  $q_{\text{las.r}} = A q_0 \exp(-kr^2)$ ,  $r^2 = (x_{\text{cent}}^2 - x^2)^2 + (x^1)^2 = (|\mathbf{V}| t - (x^2)^2)^2 + (x^1)^2$ , and  $q_i = -\lambda_{ij} \partial T / \partial x^j$ ,  $i, j = 1, 2, 3$ ,  $i = j$ .

By applying the procedure of the finite-element method in the form of the Bubnov–Galerkin method (integral formulation of the finite-element method) to the heat-conduction equation (1) and to boundary conditions (3), we can obtain [4] the matrix equation of heat balance of an ensemble of finite elements

$$[C] \{\dot{T}\} + [\Lambda] \{T\} = \{Q\}, \quad (4)$$

in which the thermophysical characteristics of a material as functions of the temperature are taken into account. Therefore, it determines a system of nonlinear ordinary differential equations of first order to solve which we will employ the numerical algorithm [1] constructed on the basis of the two-layer difference scheme [4] and the Newton method [5] and the conjugate-gradient (Lanczos) method [6].

**Calculation Results.** The algorithms of the finite-element method were realized in the C++ programming language in the form of a program for the MS Windows 2000 operating system with the use of the Borland C++ Builder 5 source development environment for Windows applications. The program represents an interface written for the MS Windows 2000 operating system with the use of a standard library of visual components of the Borland C++ Builder 5 environment; the interface includes modules (in the form of corresponding h- and cpp-files) realizing the object code of the finite-element analysis of the problem of heat conduction in laser heating.

The characteristics of the calculation region are presented in Table 1. In the calculation, we employed the following values of the parameters: initial temperature of the body 293 K, average power of laser radiation 500 W, linear velocity of travel of the beam 8 m/min, diameter of the heating spot 3 mm, coefficient of surface heat transfer 10 W/(m<sup>2</sup>·K), effective coefficient of radiation 0.9, effective coefficient of absorption of the surface 0.9, and temperature of the ambient medium 293 K. A two-level implicit difference scheme was employed in solution. The error of both the Newton and Lanczos methods was characterized by the norm of the residual vector of nodal values of the temperature. In both cases we took it to be 0.1 K. Figure 2 shows the distribution of the temperature field on the surface of the calculation region at different instants of time and different stages of the process of formation of the heat-affected zone that correspond to them.

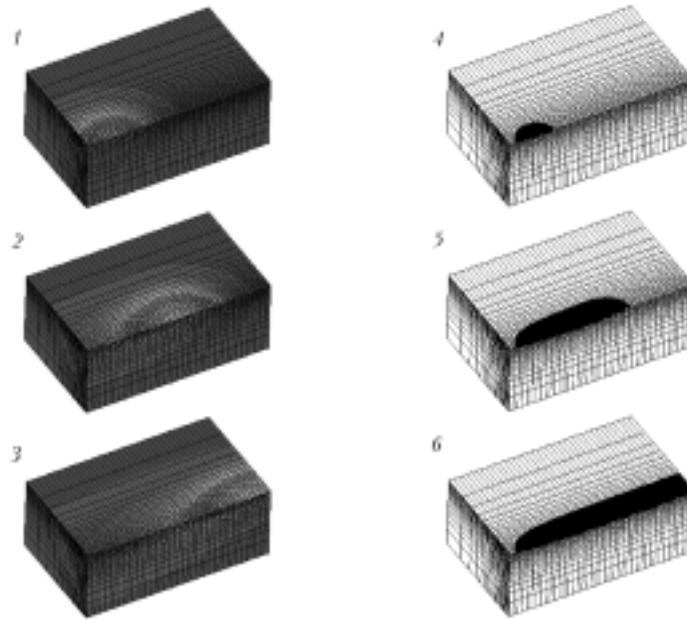


Fig. 2. Distribution of the temperature field over the surface of the calculation region (1, 2, 3) and process of formation of the heat-affected zone (4, 5, 6) at different instants of time, sec: 1 and 4)  $7.5 \cdot 10^{-3}$ ; 2 and 5)  $2.25 \cdot 10^{-2}$ ; 3 and 6)  $3.75 \cdot 10^{-2}$ .

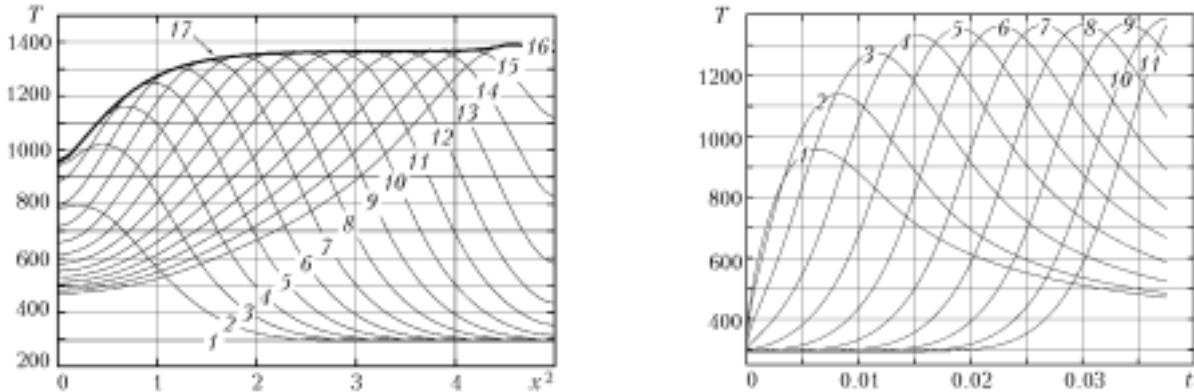


Fig. 3. Distribution of the temperature field along the coordinate direction  $x^2$  at different instants of time, sec: 1) 0; 2)  $2.5 \cdot 10^{-3}$ ; 3)  $5 \cdot 10^{-3}$ ; 4)  $7.5 \cdot 10^{-3}$ ; 5)  $1 \cdot 10^{-2}$ ; 6)  $1.25 \cdot 10^{-2}$ ; 7)  $1.5 \cdot 10^{-2}$ ; 8)  $1.75 \cdot 10^{-2}$ ; 9)  $2 \cdot 10^{-2}$ ; 10)  $2.25 \cdot 10^{-2}$ ; 11)  $2.5 \cdot 10^{-2}$ ; 12)  $2.75 \cdot 10^{-2}$ ; 13)  $3 \cdot 10^{-2}$ ; 14)  $3.25 \cdot 10^{-2}$ ; 15)  $3.5 \cdot 10^{-2}$ ; 16)  $3.75 \cdot 10^{-2}$ ; 17) curve of the maximum values.  $T$ , K;  $x^2$ , mm.

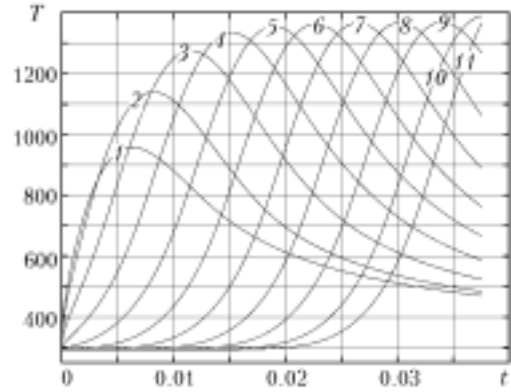


Fig. 4. Family of thermal cycles of the points distributed along the coordinate direction  $x^2$ , mm: 1) 0; 2) 0.5; 3) 1.0; 4) 1.5; 5) 2.0; 6) 2.5; 7) 3.0; 8) 3.5; 9) 4.0; 10) 4.5; 11) 5.0.  $T$ , K;  $t$ , sec.

The position of the heat-affected zone was evaluated as a first approximation by the isotherm  $T = 1000$  K, which corresponds to the point of polymorphous phase  $\alpha \leftrightarrow \gamma$  transition on the equilibrium diagram Fe-C [1]. Thus, the heat-affected zone involves all the points of the calculation region the peak value of the thermocycle at which is no lower than 1000 K.

For the technology of laser hardening it is of interest to consider the characteristics of a certain cross section  $x^2 = \text{const}$  that falls within the zone of the quasistationary regime of heating for the reason that other such cross sections that are at a rather large distance from the edges of the calculation region along the  $x^2$  axis will be characterized analogously.

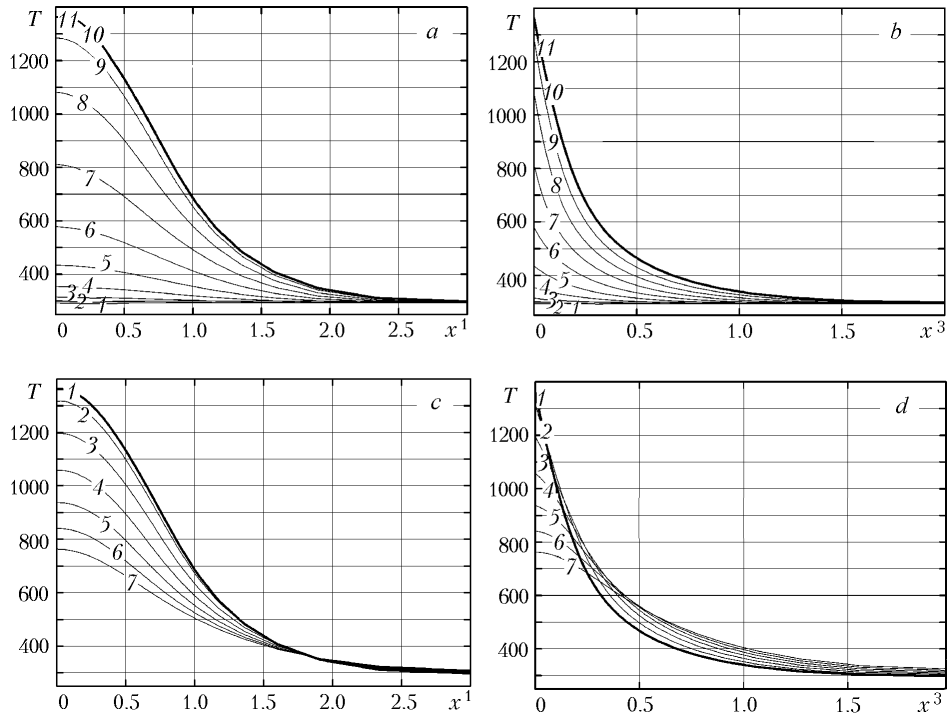


Fig. 5. Distribution of the temperature field in the cross section  $x^2 = 3$  mm in the stage of heating (a, b, 1–11) and cooling (c, d, 1–7) over the height (a, c) and the width (b, d) at different instants of time, sec: 1) 0; 2)  $2.5 \cdot 10^{-2}$ ; 3)  $5 \cdot 10^{-3}$ ; 4)  $7.5 \cdot 10^{-3}$ ; 5)  $1 \cdot 10^{-2}$ ; 6)  $1.25 \cdot 10^{-2}$ ; 7)  $1.5 \cdot 10^{-2}$ ; 8)  $1.75 \cdot 10^{-2}$ ; 9)  $2 \cdot 10^{-2}$ ; 10)  $2.25 \cdot 10^{-2}$ ; 11)  $2.27 \cdot 10^{-2}$ , limiting heating curve (in the stage of heating); 1)  $2.27 \cdot 10^{-2}$ ; 2)  $2.25 \cdot 10^{-2}$ ; 3)  $2.75 \cdot 10^{-2}$ ; 4)  $3 \cdot 10^{-2}$ ; 5)  $3.25 \cdot 10^{-2}$ ; 6)  $3.5 \cdot 10^{-2}$ ; 7)  $3.75 \cdot 10^{-2}$  (in the stage of cooling).  $T$ , K;  $x^1$  and  $x^3$ , mm.

Figure 3 shows the distribution of the temperature field at different instants of time along the coordinate direction  $x^2$  on which we observe a quasistationary regime of heating: the difference in the peak values of the thermocycles of the points lying on the coordinate axis  $x^2$  (Fig. 4) in the interval  $2.53 \text{ mm} \leq x^2 \leq 3.78 \text{ mm}$  does not exceed 6 K. The minimum value is observed at the point  $x^2 = 2.55 \text{ mm}$  and is 1361.5 K, while the maximum value is observed at the point  $x^2 = 3.75 \text{ mm}$  and is equal to 1367.4 K for an average peak value of 1364.5 K. The inconsistency between the minimum value of the temperature and the left-hand limit of the interval selected and between the maximum value and the right-hand limit is attributed to the computational error, which, however, is small.

Let us investigate the cross section that falls within the zone of quasistationary heating and that is at a rather large distance from both ends of the calculation region along the coordinate direction  $x^2$ . We select  $x^2 = 3 \text{ mm}$  as such a cross section.

The temperature-field distribution over the width of the cross section in question (along the vector  $\overline{\{3, 0, 0\}}$  with the origin at the point  $(0, 3, 0)$ ) is shown in Fig. 5a for the heating stage and in Fig. 5c for the cooling stage. In these figures, we can track the time change in the extent of the heat-affected zone of this cross section along the coordinate direction  $x^1$  (its width) and can determine its final value as the maximum abscissa of those of the points of intersection of the isotherm  $T = 1000 \text{ K}$  and the temperature-distribution curves. Proceeding in this manner, we find that the width of the heat-affected zone is equal to  $\approx 653 \mu\text{m}$ .

The temperature-field distribution over the height of the cross section in question (along the vector  $\overline{\{0, 0, 2\}}$  with the origin at the point  $(0, 3, 0)$ ) is shown in Fig. 5b for the heating stage and in Fig. 5d for the cooling stage. In these figures, we can analogously track the time change in the extent of the heat-affected zone of this cross section along the coordinate direction  $x^3$  (its height) and can determine its final value, which was  $\approx 123 \mu\text{m}$ .

The extent of the heat-affected zone of the cross section in question along the directions  $x^1$  (over the width) and  $x^3$  (over the height) can be determined by analyzing thermal cycles at the points (Fig. 6) that lie along the vectors

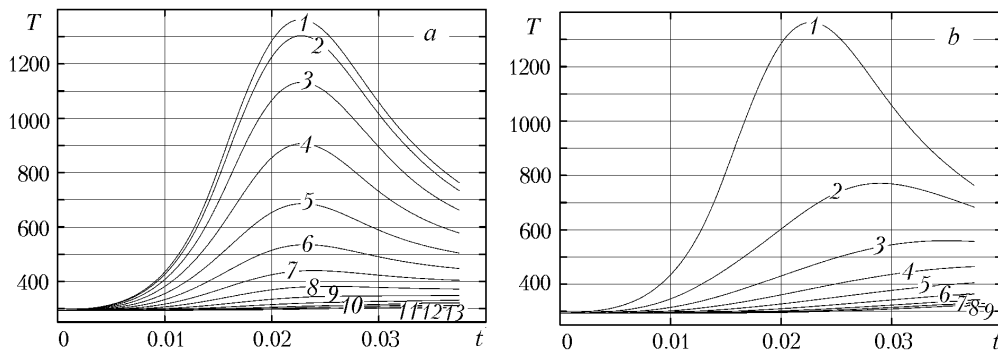


Fig. 6. Family of thermal cycles of the points distributed over the width (a) and height (b) of the cross section  $x^2 = 3$  mm: 1) 0; 2)  $2.5 \cdot 10^{-1}$ ; 3)  $5 \cdot 10^{-1}$ ; 4)  $0.75 \cdot 10^{-1}$ ; 5) 1.0; 6) 1.25; 7) 1.5; 8) 1.75; 9) 2.0; 10) 2.25; 11) 2.5; 12) 2.75; 13) 3.0.  $T$ , K;  $t$ , sec.

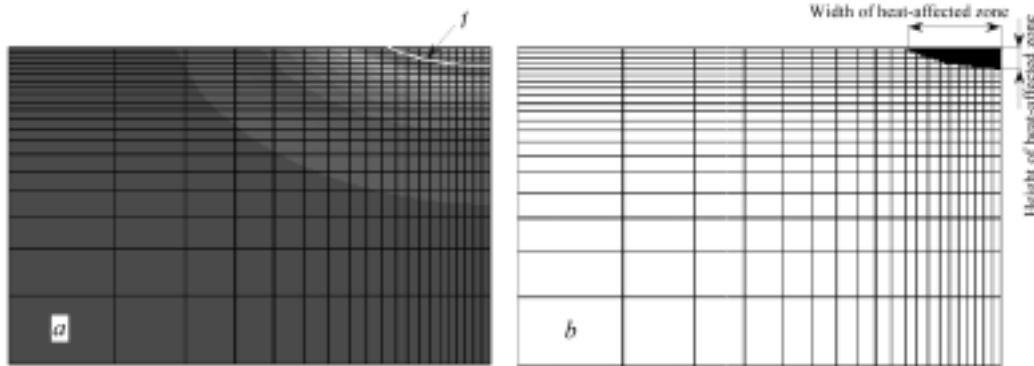


Fig. 7. Distribution of the temperature field (a) over the cross section  $x^2 = 3$  mm at the instant of time  $t = 2.27 \cdot 10^{-2}$  sec [1] isotherm 1000 K] and geometry of its heat-affected zone (b).

determined above: at the points determining the boundaries of the cross-sectional heat-affected zone, the peak values of the thermal cycles are equal to 1000 K.

Based on Figs. 4 and 6, we can estimate the average rates of heating and cooling for the cross section  $x^2 = 3$  mm. For the points lying within the heat-affected zone of the cross section in question the average rate of heating was  $4.99 \cdot 10^5 - 0.93 \cdot 10^6$  K/sec while the average rate of cooling was  $5.09 \cdot 10^4 - 1.59 \cdot 10^4$  K/sec. The calculated results obtained are in good agreement with experimental data [7], which determine the interval of the rates of heating and cooling as  $10^5 - 10^6$  K/sec and  $10^4 - 10^5$  K/sec respectively.

The temperature-field distribution over the cross section  $x^2 = 3$  mm at the instant of time  $t = 2.27 \cdot 10^{-2}$  sec corresponding to the peak value of a thermocycle at the point (0, 3, 0) is given in Fig. 7a, and the geometry of the heat-affected zone of the cross section in question is shown (in black) in Fig. 7b.

Analyzing the data in Fig. 5, we can infer that with the prescribed scheme of thermal loading for a cross section that falls within the zone of quasistationary heating the temperature change over the height of the cross section significantly exceeds the temperature change over its width. This is a consequence of the action of the heat-conduction mechanism under different conditions: the cross section is subjected to heating over the width, whereas the action of the heat sources over the height is absent. Thus, at the boundary of the heat-affected zone in the  $x^3$  direction, there is a "cold" metal, which contributes to a more intense removal of heat from the heat-affected zone in this direction.

The maximum time of stay above the temperature of the  $\alpha \leftrightarrow \gamma$  transition for the cross section selected is observed at the point (0, 3, 0) and is  $1.45 \cdot 10^{-2}$  sec. This time decreases as the boundary of the heat-affected zone is approached, and it becomes equal to zero behind the boundary. The value of the time of stay is of primary importance in the formation of the final structure of steel and its properties — it limits the diffusion processes of austenization and homogenization in the stage of heating. Since we observe thermocycles having generally different times of stay

above the temperature of the  $\alpha \leftrightarrow \gamma$  transition at the points of the cross section with such a thermal-loading scheme and the peak value and the heating and cooling rates, the final structure and properties of the hardened steel in the heat-affected zone are spatially nonuniform.

Thus, the results of the calculations show that the thermal cycles obtained of the points within the heat-affected zone of the cross section  $x^2 = \text{const}$  that falls within the zone of the quasistationary regime of heating possess the features of laser thermocycles, which are characterized by high heating and cooling rates, a high peak value of the temperature, and a short time of stay above the temperature of the  $\alpha \leftrightarrow \gamma$  transition.

## NOTATION

$c_v$ , specific heat at constant volume,  $\text{J}/(\text{m}^3 \cdot \text{K})$ ;  $\rho$ , density,  $\text{kg}/\text{m}^3$ ;  $T$ , temperature,  $\text{K}$ ;  $t$ , time,  $\text{sec}$ ;  $\lambda$ , thermal-conductivity tensor;  $x^i$ ,  $i$ th, coordinate direction (axis);  $\lambda_{ij}$ , component of the thermal-conductivity tensor;  $T_0$ , initial temperature of the body,  $\text{K}$ ;  $\mathbf{V}$ , vector of the linear velocity of travel of the laser beam,  $[\mathbf{V}] = \text{m}/\text{sec}$ ;  $q_i$ , specific flux (density),  $\text{W}/\text{m}^2$ ;  $q_{\text{conv}}$ ,  $q_{\text{rdnt}}$ , and  $q_{\text{las.r}}$ , specific fluxes (densities) reflecting the convective and radiant modes of heat exchange and laser heating respectively,  $\text{W}/\text{m}^2$ ;  $L_i$  ( $i = 1, 2, 3$ ), linear dimension of the calculation region (in the shape of a parallelepiped) along the  $i$ th coordinate direction,  $\text{m}$ ;  $\alpha(x^i, T)$ , coefficient of surface heat transfer,  $\text{W}/(\text{m}^2 \cdot \text{K})$ ;  $T_{\text{amb.med}}$ , temperature of the ambient medium,  $\text{K}$ ;  $\varepsilon$ , effective coefficient of radiation of the heated surface, dimensionless quantity;  $\sigma$ , Stefan–Boltzmann constant,  $5.67051(19) \cdot 10^{-8} \text{ W}/(\text{m}^2 \cdot \text{K}^4)$ ;  $A$ , absorption coefficient of the surface, dimensionless quantity;  $q_0$ , maximum value of the density of the flux from laser radiation,  $\text{W}/\text{m}^2$ ;  $k$ , concentration coefficient of normal distribution,  $\text{m}^{-2}$ ;  $r$ , distance from the center of the heating spot with coordinates  $(0, x_{\text{cent}}^2, 0)$  to the point with coordinates  $(x^1, x^2)$  on the surface of the body  $x^3 = 0$ ;  $x_{\text{cent}}^1 = \text{const} = 0$  and  $x_{\text{cent}}^2 = \text{var} = |\mathbf{V}|t$ , coordinates of the center of the laser-heating spot,  $\text{m}$ ;  $q_i = -\lambda_{ij} \partial T / \partial x^j$ , flux densities from the Fourier heat-conduction law,  $\text{W}/\text{m}^2$ ;  $[C]$ , global heat-capacity matrix,  $\text{J}/\text{K}$ ;  $[\Lambda]$ , global conduction matrix,  $\text{W}/\text{K}$ ;  $[Q]$ , global matrix of generalized concentrated heat fluxes,  $\text{W}$ ;  $\{\dot{T}\}$ , column matrix of nodal values of the derivatives of temperature with respect to time,  $\text{K}/\text{sec}$ ;  $\{T\}$ , column matrix of nodal values of the temperature,  $\text{K}$ ;  $\alpha \leftrightarrow \gamma$ , notation of the structural polymorphous eutectoid phase transition in iron-based alloys; Fe–C, notation of the "iron–carbon" phase diagram of state of Fe-based alloys in coordinates  $(T, c)$ : temperature, concentration of carbon in the alloy;  $\Delta t$ , value of the time interval,  $\text{sec}$ . Subscripts: las.r, laser radiation; conv, convective; rdnt, radiant; amb.med, ambient medium; cent, center.

## REFERENCES

1. E. I. Degtyarev and G. N. Kuvyrkin, in: *Sci. Papers presented at the IVth Int. Seminar "Modern Problems of Strength" dedicated to V. A. Likhachev* [in Russian], Vol. 1, Novgorod, Staraya Russa (2000), pp. 229–234.
2. E. I. Degtyarev, in: *Sci. Papers presented at the Vth Int. Seminar "Modern Problems of Strength" dedicated to V. A. Likhachev* [in Russian], Vol. 1, Novgorod, Staraya Russa (2001), pp. 288–293.
3. G. N. Kuvyrkin, in: *Thermomechanics of a Deformable Rigid Body under Highly Intense Loading* [in Russian], Moscow (1993), pp. 97–105.
4. V. S. Zarubin and V. V. Selivanov, in: *Variational Methods of the Mechanics of a Continuum* [in Russian], Moscow (1993), pp. 250–258.
5. A. A. Amosova, Yu. A. Dubinskii, and N. V. Kopchenova, in: *Computational Methods for Engineers* [in Russian], Moscow (1994), pp. 201–204.
6. G. Golub and C. Van Loan, in: *Matrix Calculations* [Russian translation], Moscow (1999), pp. 433–442.
7. E. A. Shcherbakova, *Development of the Computational Technique for Predicting the Structure in Laser Quenching of Carbon Steels in Order to Choose Rational Regimes of Strengthening of Component Parts*, Candidate's Dissertation (in Engineering), Moscow (1993).